Structural Engineering and Mechanics, *Vol. 54, No. 1 (2015) 1-17*
DOI: http://dx.doi.org/10.12989/sem.2015.54.1.001

Behavior and crack development of fiber-reinforced concrete spandrel beams under combined loading: an experimental study

Omer Farouk Ibraheem[a], B.H. Abu Bakar* and I. Johari[b]

Department of Civil Engineering, University Sains Malaysia (USM), Penang, Malaysia

(Received October 11, 2013, Revised March 17, 2014, Accepted August 31, 2014)

Abstract. An experimental investigation is conducted to examine the behavior and cracking of steel fiber-reinforced concrete spandrel L-shaped beams subjected to combined torsion, bending, and shear. The experimental program includes 12 medium-sized L-shaped spandrel beams organized into two groups, namely, specimens with longitudinal reinforcing bars, and specimens with bars and stirrups. All cases are examined with 0%, 1%, and 1.5% steel fiber volume fractions and tested under two different loading eccentricities. Test results indicate that the torque to shear ratio has a significant effect on the crack pattern developed in the beams. The strain on concrete surface follows the crack width value, and the addition of steel fibers reduces the strain. Fibrous concrete beams exhibited improved overall torsional performance compared with the corresponding non-fibrous control beams, particularly the beams tested under high eccentricity.

Keywords: reinforced concrete; torsion; combined loading; spandrel beam; steel fiber; crack

1. Introduction

The development of cracks, the nature of their deployment, and the areas of concentration clearly exhibit the type of loads that affect the structure and the expected type of failure and origin. Determining where failure occurs in the structural member is important to find ways to strengthen the member externally, such as by using carbon fiber reinforced polymer, or internally, such as by adding certain materials to the concrete mix (e.g., steel fibers). Crack widths are also a good indicator of the structure state. They should be observed to determine whether the structure stability is satisfactory. Crack widths in reinforced concrete structures largely affect structural performance, such as shear, tensile, and bending stiffness, energy absorption capacity, ductility, and corrosion resistance of reinforcement. Excessive cracks caused by either or both restrained deformation and external loads are the most common causes or damage in concrete structures that result in huge annual cost to the construction industry. Actually, crack growth and widths are

∗Corresponding author, Professor, E-mail: cebad@usm.my
[a]Ph.D., E-mail: omer.eng2011@yahoo.com
[b]Ph.D.

Copyright © 2015 Techno-Press, Ltd.
http://www.techno-press.org/?journal=sem&subpage=8 ISSN: 1225-4568 (Print), 1598-6217 (Online)

inherently subject to wide scatter even in careful laboratory work. They are influenced by shrinkage and other time-dependent effects.

The addition of steel fibers in concrete mixture has long been recognized as a non-conventional mass reinforcement that enhances the mechanical properties of concrete and provides a means for controlling crack propagation (ACI 318 1999). This ability is attributed to the tensile stress transfer capability of steel fibers across crack surfaces, known as crack-bridging, and to the fact that such fibers provide significant resistance to shear across developing cracks (Newman and Choo 2003).

Torsional failure of concrete members is initiated by tensile stress which developed as a result of a state of pure shear, which arose because of torsion (Hsu 1984). Under combined loading, tensile stresses and crack width may increase, thus leading to sudden failure of the concrete member.

The research on the torsional behavior of fibrous concrete members during the last three decades can be classified into two main parts. The first part is the behavior of fibrous concrete members under pure torsion, which accounts for a large share of the experimental research on the torsional behavior of SFRC beams. Experiment of works have been conducted on fibrous beams without steel reinforcement (Mansur and Paramasivam 1982, Craig *et al.* 1986, Wafa *et al.* 1992, Gunneswara Rao and Rama Seshu 2003), with longitudinal reinforcement only (Chalioris and Karayannis 2009), and with longitudinal and transverse reinforcements (Narayanan and Kareem 1986, El-Niema 1993, Gunneswara Rao and Rama Seshu 2005, Okay and Engin 2012).

All of these experimental studies have provided insight into the torsional response of fiber-reinforced concrete beams under pure torsion and have concluded that the addition of steel fibers improves the torsional behavior and cracking characteristics of concrete beams.

The second part is the behavior of SFRC beams under combined loading. Published works on fiber-reinforced concrete members under combined loading (torsion–shear, torsion–bending, and torsion–bending–shear) are scarcely available. A previous study focused on investigating the behavior of fibrous beams without steel reinforcement (Mansur and Paramasivam 1985), whereas another research conducted the effect of transverse reinforcements on fibrous members (Avinash and Parekar 2010).

All of the abovementioned works have studied the behavior of rectangular cross-sectional fibrous beams. The published work for flanged fibrous concrete beams is relatively limited and has been mainly conducted by the authors (Chalioris and Karayannis 2009).

The research on the behavior of flanged fibrous concrete beams under combined torsion, bending, and shear is almost nonexistent.

This lack of research may be attributed to the complex nature of these members; nonetheless, such complexity, which can be found in sensitive locations within the structural buildings as in the case of edge beams, is important.

Spandrel beams located at the perimeters of buildings carry loads from slabs, joists, and beams from one side of the member only. This loading mechanism generates torsional forces that are transferred from the spandrel beams to the columns. These beams do not fail only under the influence of torsional loads; other loads are accompanied by torsional loads, such as bending, torsion and sometimes, even shear. End beams with slabs on only one side will have a typical L-shape, from which the name “L-beam” was derived (Wight and Macgregor 2009). An L-beam is also called a spandrel or edge beam. The aforementioned loads, along with the non-symmetric shape, result in this type of beams falling under the influence of a complex combination of stresses, which explain the limited number of studies on this subject.

In the present investigation, 12 L-shaped reinforced concrete spandrel beams with steel fibers were tested under combined torsion-bending-shear at different values of eccentricities, torsion-to-shear ratio (T/V), and different steel reinforcement cases.

2. Experimental program

The experimental program included 12 L-shaped spandrel beams tested under combined torsion, bending, and shear, and sorted into two groups based on conventional steel reinforcements. Tested beams were constructed using plain concrete (control specimens) and steel fiber concrete with 1.0% and 1.5% volume fractions of fibers.

2.1 Materials

The concrete mix consisted of ordinary Portland cement, river sand with a fineness modulus of 2.6, and coarse aggregate with a maximum size of 19.5 mm.

The concrete mixture was made using cement, sand, and crushed aggregate with a mixture proportion of 1:2:2.5 and a water cement ratio of 48%, which remained constant and identical for all test beams so that the only variable was the steel fiber content. The mixture was designed to have a specified 28-day strength of 40.0 MPa.

The prepared fresh fibrous concrete mixture was carefully placed in molds for the specimens and vibrated for a sufficient period by a portable electrical vibrator to ensure suitable consolidation of the mixture. Concrete test cubes and cylinders were cast simultaneously with the test beams for each mixture and vibrated using a frequency-vibrating table. The average concrete strength values of the tested beams are presented in Table 1. The code names of the tested beams comprise three parts. The first part represents the beam reinforcement case: longitudinal reinforcement only (L), and longitudinal and stirrups (S). The second part represents the steel fiber volume ratio: 0%, 1%, and 1.5%. The third part represents the load eccentricities, that is, 545 mm and 145 mm.

Table 1 Material properties of the tested beams

Group No.	Beam Name	Volume of steel fiber (%)	Compressive Strength at 28 days (MPa)	Split Tensile Strength at 28 days (MPa)
I	L0-145	0	41.2	3.0
I	L1-145	1.0	43.0	5.7
I	L1.5-145	1.5	46.0	5.9
I	L0-545	0	38.2	2.8
I	L1-545	1.0	46.0	6.3
I	L1.5-545	1.5	42.2	7.1
II	S0-145	0	43.3	3.3
II	S1-145	1.0	44.0	5.5.
II	S1.5-145	1.5	41.4	6.1
II	S0-545	0	42.8	2.7
II	S1-545	1.0	41.0	5.0
II	S1.5-545	1.5	35.5	6.0

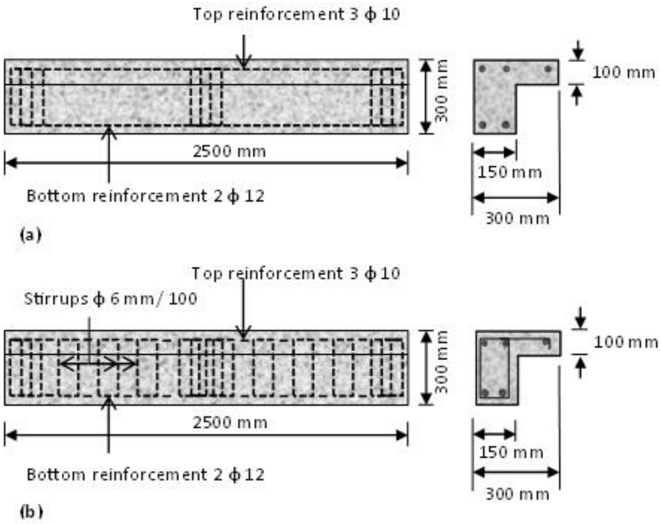

Fig. 1 Elevation, cross-sectional dimensions, and steel reinforcement details of the tested beams: (a) Group I, (b) group II

Bent-ended steel fibers with aspect ratios l_f/d_f =60/0.75=80 were used, where l_f denotes fiber length and d_f denotes fiber diameter. Two steel fiber volume fractions, V_f, were adopted, namely: (1) a moderate one equal to 1% or 78.5 kg per 1 m^3 concrete and (2) a ratio limited by practical considerations in structural members equal to 1.5% or 117.75 kg per 1 m^3 concrete (Wight and Macgregor 2009). The average yield strength of the steel fibers provided by the manufacturer was f_{yf} =1100 MPa (±100 MPa).

The average yield strength of the steel reinforcement was 420, 570, and 450 MPa for a diameter of 12, 10, and 6 mm, respectively.

2.2 Tested beams

Twelve identical reinforced concrete spandrel beams were built. The beams were 2500 mm long with an L-shaped cross section. The 100 mm×150 mm flange represented a section of the floor slab at the perimeter of an reinforced concrete diaphragm. Tested beams were sorted into two groups based on their conventional steel reinforcement. The first group included six beams with longitudinal reinforcement only, and the second group included beams with longitudinal reinforcement and stirrups.

The beams of the first group were reinforced with longitudinal bars (2ϕ 12 mm) at the bottom and (3ϕ10 mm) at the top. The beams of the second group had the same longitudinal reinforcement details as group one beams with the addition of stirrups (ϕ 6 mm/100 mm). All beams were over-reinforced at the ends and at mid span to avoid concrete crushing because of stress concentration. The spandrel beam specimens were manufactured according to the design guidelines outlined in ACI code (ACI 318-2005). Dimensions and reinforcement details of tested beams are shown in Fig. 1.

2.3 Test setup

The specimens were allowed to rest at the ends on L-shaped steel supports over a constant span of 2200 mm. The supports did not permit horizontal movement, vertical movement, and rotation around the beam axis. At mid span, a lever arm of an I-section steel beam was attached to the top face of the beam and tightly bolted around the spandrel beam (Fig. 2). A hydraulic compressor with a 450 kN capacity was applied on the lever arm at any eccentricity (e) to achieve the required torque-to-shear (eccentricity) ratio. The applied vertical load caused vertical reactions and torques at the end supports and induced internal torque, bending moment, and shear force in the specimens, as shown in Fig. 3. The load was imposed at a constant load step and measured by a load cell with an accuracy equal to 0.05 kN. The average angle of twist and vertical displacement at mid span of the tested beams were measured using the measurements of a set of linear variable displacement transducers (LVDT) with an accuracy of 0.02 mm placed along the steel arm, as shown in Fig. 2. To capture each significant detail of the behavior of the specimens, constant load steps were selected for each group.

A crack detection microscope was used to measure the width of the crack that developed on the concrete surfaces of all specimens. The 4mm range of measurement has a lower scale with 0.2 mm divisions. These 0.2 mm divisions were further subdivided into 0.02 mm divisions (Fig. 4).

Fig. 2 Test rig, LVDT distribution and support detail

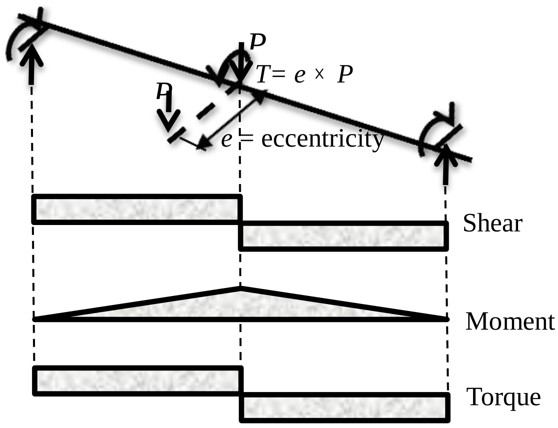

Fig. 3 Shear, moment and torque diagrams

Fig. 4 Crack detection microscope

Table 2 Summary of the results

Group No.	Beam Name	Cracking Load (kN)	Cracking Torque (kN.m)	Max. Load (kN)	Max. Torque (kN.m)	$\theta cr.$ (rad)	θmax. (rad)	$\Delta cr.$ (mm)	Δmax. (mm)
1	L0-145	16	1.16	45.3	3.28	0.0012	0.0176	1.2	11.00
1	L1-145	26	1.88	63.4	4.60	0.0015	0.0200	1.9	24.75
1	L1.5-145	30	2.18	71.0	5.15	0.0015	0.0250	2.3	38.00
1	L0-545	14	3.82	29.0	7.90	0.0080	0.0700	1.5	6.80
1	L1-545	22	6.00	45.0	12.26	0.0100	0.1300	2.2	10.70
1	L1.5-545	30	8.18	53.0	14.44	0.0130	0.1460	3.1	13.40
2	S0-145	15	1.09	49.5	3.59	0.0012	0.0136	1.2	18.68
2	S1-145	23	1.67	70.0	5.08	0.0016	0.0280	1.8	41.30
2	S1.5-145	28	2.03	76.0	5.51	0.0018	0.0296	2.0	49.00
2	S0-545	12	3.27	38.0	10.36	0.0070	0.1230	1.1	10.10
2	S1-545	19	5.18	50.0	13.63	0.0080	0.1690	1.8	20.50
2	S1.5-545	25	6.81	59.1	16.11	0.0140	0.2150	3.2	32.60

3. Test results and discussion

All specimens were tested under two different eccentricities: e=545 mm (that is, torsion control) and e=145 mm (that is, bending moment control). The results of the tests are presented in Table 2, including cracking load, cracking moment, maximum load, maximum moment, and the corresponding rotation and deflection at mid span for all groups.

3.1 Torsional strength

For the beams in Group I, the plain specimens (without steel fiber) demonstrate an increasing post-cracking response compared with that under pure torsion. Beams with longitudinal reinforcement did not exhibit an increase in post-cracking response under pure torsion (Chalioris

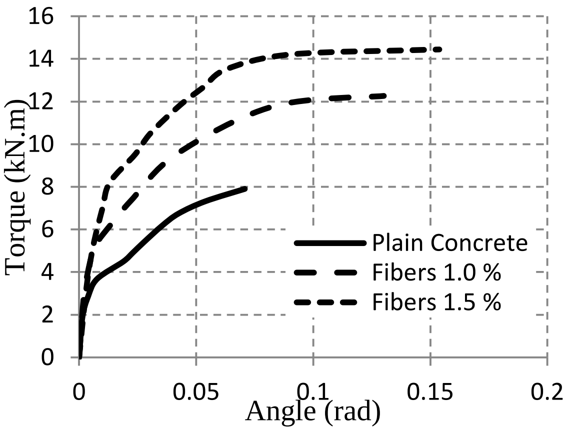

Fig. 5 Torque-twist curve for the beams in Group I at *e*=545 mm

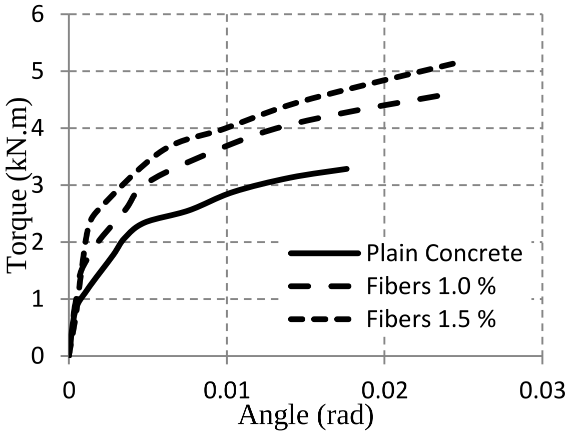

Fig. 6 Torque-twist curve for the beams in Group I at *e*=145 mm

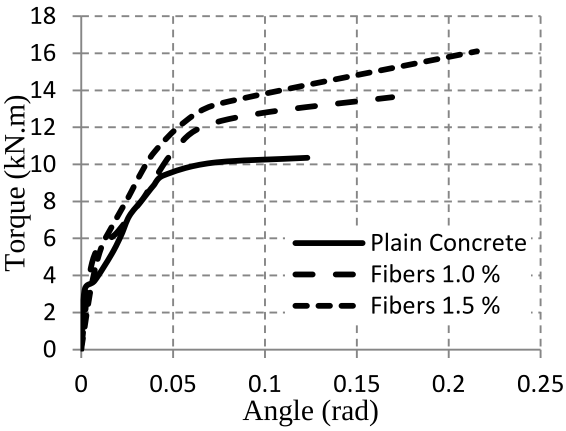

Fig. 7 Torque-twist curve for the beams in Group II at *e*=545 mm

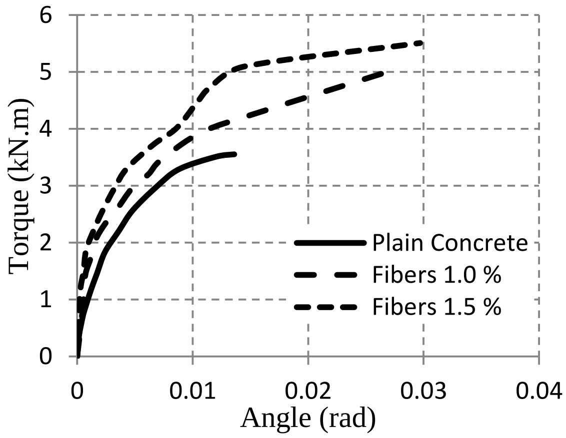

Fig. 8 Torque-twist curve for the beams in Group II at *e*=145 mm

and Karayannis 2009). This result can be attributed to the interaction of the beams with shear force and bending moment, as well as the contribution of the reinforced flange due to the increase in the torsional strength of these beams after torsional cracking (Zararis and Penelis 1986).

Instead of common stirrups, steel fibers can be used as shear reinforcement by adding an adequate percentage of steel fibers. Moreover, the post-cracking response increased at high fiber percent ratio, particularly for specimens under high torsion (see Tables 2). Fig. 5 shows that at eccentricity=545 mm, a 55.2% and 82.7% increase was observed after adding steel fibers with a volume of 1% and 1.5%, respectively.

At a low eccentricity value (*e*), the bending moment will be controlled so that the post-cracking response is already increasing. An 57.0% increase in strength was noted after the addition of 1.5% steel fibers, as shown in Fig. 6.

The effectiveness of steel fibers in increasing the tensile strength of the concrete, at least, partially, depends on the number of fibers per unit cross-sectional area of concrete. In specimens under high eccentricity (high torsion), a large area of cross-section will be under tensile stresses, so that the strength of specimens can be better observed during torsion control than during high bending moment.

The existence of transverse reinforcements in spandrel beams will increase torsional strength at high eccentricity value for the beams of Group II. Thus, as shown in Fig. 7 and Fig. 8, the addition of steel fibers affecting the strength compared with that on the specimens of Groups I. Although steel fibers were added, the behavior of the beams was affected primarily by stirrups, as observed by Avinash and Parekar (2010). Increases of 31.6% and 55.5% were observed, respectively, after adding 1% and 1.5% steel fibers at e=545 mm. At e=145 mm, increases of up to 41.4% and 53.5 % were observed, respectively.

3.2 Cracking pattern

The cracking load values of the steel fiber concrete beams were higher than the corresponding values of the control specimens without fibers (Table 2). Crack propagation was observed on three faces of beams under high eccentricity and on two faces of beams under low eccentricity. These faces are back face (away from flange), flange face, and top face.

For the control specimens in Group I at e=545 mm (high torque), the first crack started at the bottom of the back side across the middle section at load level P_{cr}=0.48 $P_{\max}$, followed by a crack on the flange side at load level 0.52 $P_{\max}$. The spiral form propagation of the initial crack toward the top face of the beam when the load increased indicated the control of the torque on beam behavior (Deifalla and Ghobarah 2010). Finally, the crack on the top face of the beam appeared at $P_{\max}$, and the beam failed in torsional mode. The beam was brittle and had low ductility. Fig. 9 shows the crack propagation for L0-545 beam.

For the beam tested under e=145 mm (high bending moment), the first crack occurred at the mid-span of the beam at load level P_{cr}=0.35 $P_{\max}$ on the back and flange sides. As expected, the

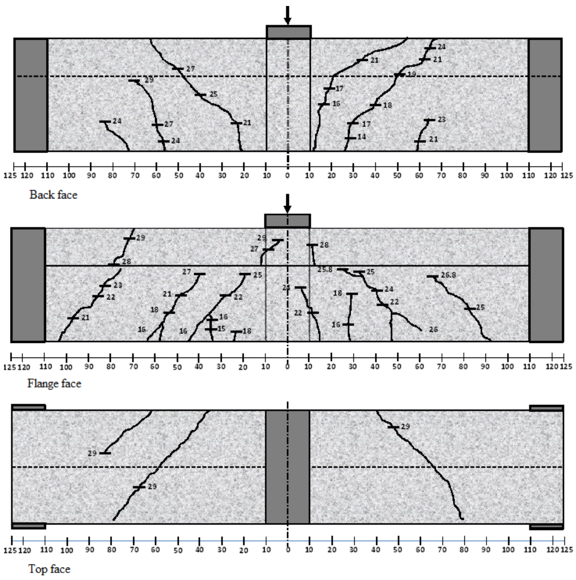

Fig. 9 Crack pattern in beam L0-545

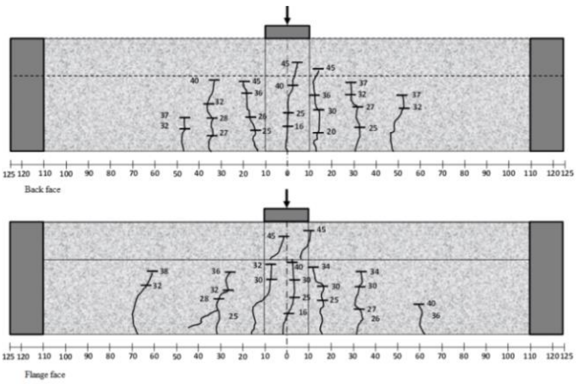

Fig. 10 Crack pattern in beam L0-145

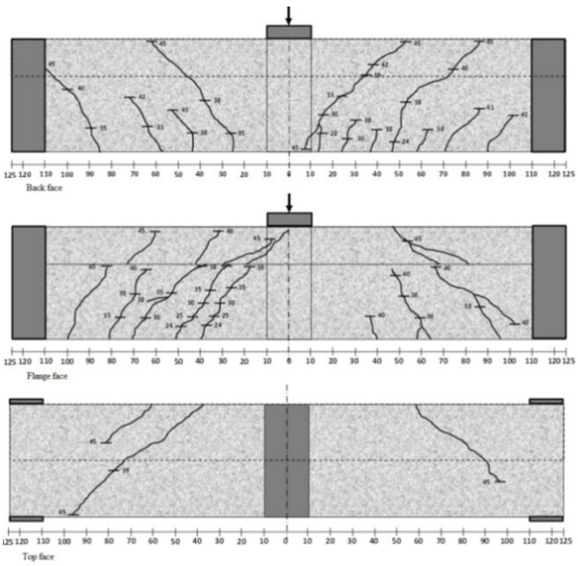

Fig. 11 Crack pattern in beam L1-545

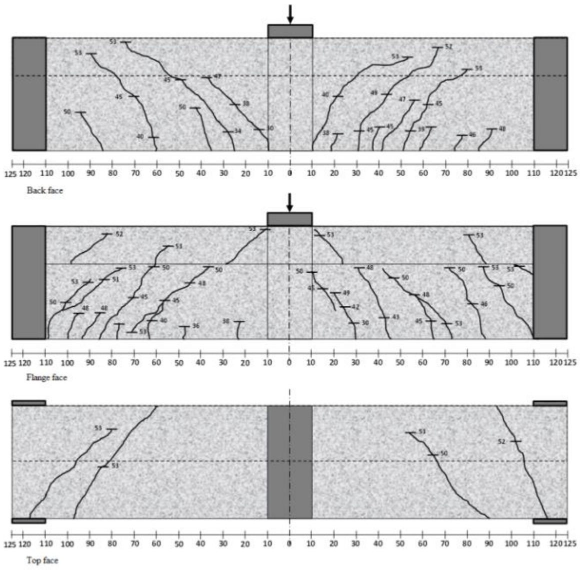

Fig. 12 Crack pattern in beam L1.5-545

initial cracks did not follow a spiral form, indicating that they were flexural cracks and that the beam failed in the flexural mode (Fig. 10 for beam L0-145).

In the two loading cases, the bars prevented the specimens from splitting into two parts. Two failure mechanisms were identified in this group. The first one is characterized by full cracking of the beam (the top face cracks) that occurs at high eccentricity value (i.e., when torsion is controlled). The second mechanism is characterized by partial cracking of the beam (the top face does not crack) that occurs at low eccentricity value (Zararis and Penelis 1986).

The addition of steel fibers did not change the shape of the propagation of cracks, but it led to the development of dense and more cracks in the two loading cases. The beams also collapsed under two failure modes, i.e., torsional mode failure (e=545 mm) and flexural mode failure (e=145 mm).

Beam L1-545 cracked first on the back side at load level P_{cr}=0.49 $P_{\max}$ and subsequently the flange side cracked at 0.53 $P_{\max}$. The spiral crack propagated toward the top face of the specimens and at load level 0.84 $P_{\max}$. The crack developed at the top face of the beam, causing the beam to collapse under the first failure mechanism (Fig. 11).

A similar behavior was observed on the specimen reinforced by 1.5% volume fraction (L1.5-545). The back and flange sides cracked at load level P_{cr}=0.56 $P_{\max}$, and the top face cracked at 0.94 $P_{\max}$ (Fig. 12).

At lower eccentricity, beam L1-145 cracked at mid-span on two vertical sides at P_{cr}=0.41 $P_{\max}$, and beam L1.5-145 cracked at P_{cr}=0.42 $P_{\max}$. The same general behavior was also observed for the two beams before the second failure mechanism occurred (Figs. 13 and 14).

For all specimens in Group I, the same number of cracks appeared on two vertical faces of the beams (i.e., back and flange sides), especially at a lower eccentricity value.

Beams with conventional reinforcements, including bars and stirrups in Group II, exhibited the formation of a number of helical and diagonal cracks. Crack propagation, which appeared in the beams in Group I, also occurred in the beams for this group, except that more cracks were

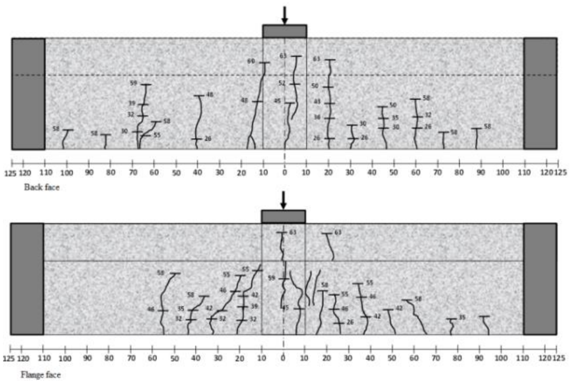

Fig. 13 Crack pattern in beam L1-145

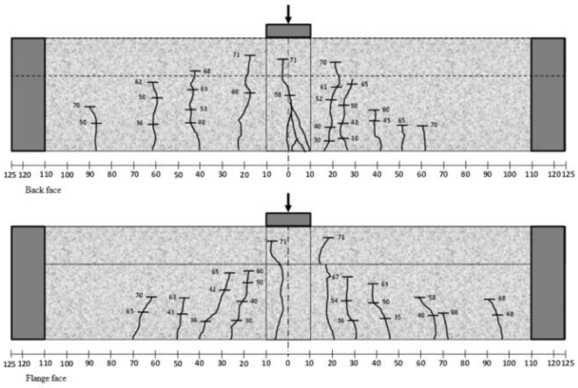

Fig. 14 Crack pattern in beam L1.5-145

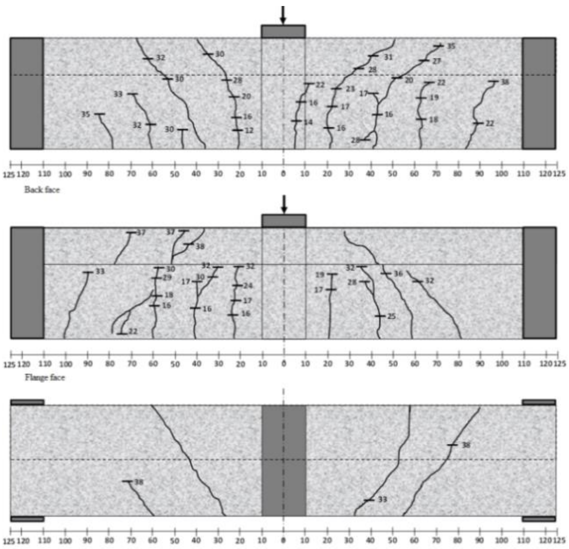

Fig. 15 Crack pattern in beam S0-545

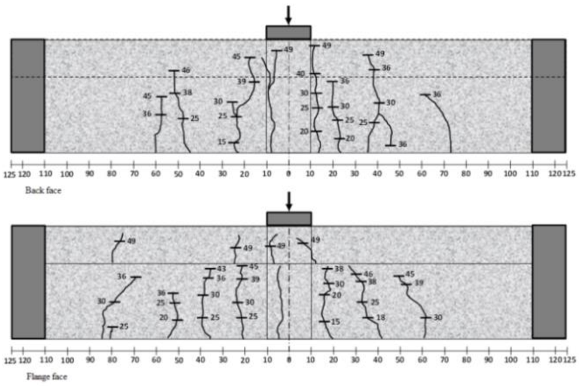

Fig. 16 Crack pattern in beam S0-145

observed in these beams than in those without stirrups. Moreover, the spaces between the cracks were closer. Beam S0-545 cracked on the back side at P_{cr}=0.32 $P_{\max}$ and subsequently crack appeared on the flange side at 0.42 $P_{\max}$. The crack on the two faces that propagated in a spiral form started at the bottom of the beam across the middle section toward the top face. The top face cracked at 0.87 $P_{\max}$ and eventually failed under torsion failure (Fig. 15).

The cracks on the two vertical faces appeared to be inclined with the horizontal axis at an angle larger than that of Group I specimens. Beam S0-145 tested under low eccentricity cracked on two vertical sides at P_{cr}=0.30 $P_{\max}$ in the vertical direction from the bottom to the top of the beam (Fig. 16).

As in the beams in group I, two failure mechanisms were also identified in this group. The full cracking of the beam (the top face cracks) occurs at a high eccentricity value (i.e., when torsion is controlled) and partial cracking of the beam (the top face does not crack) occurs at a low eccentricity value.

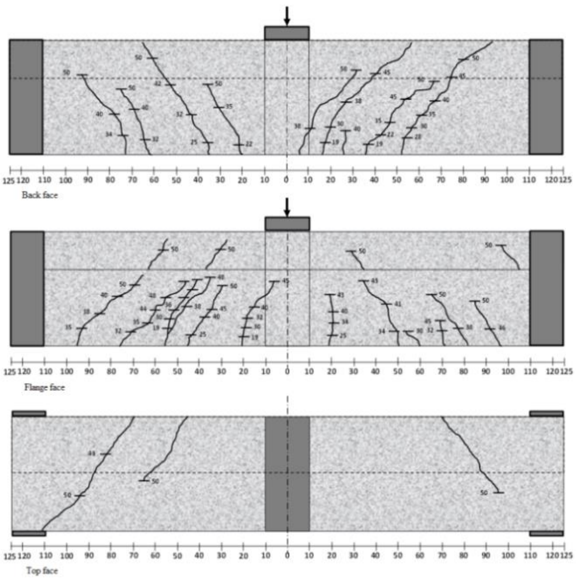

Fig. 17 Crack pattern in beam S1-545

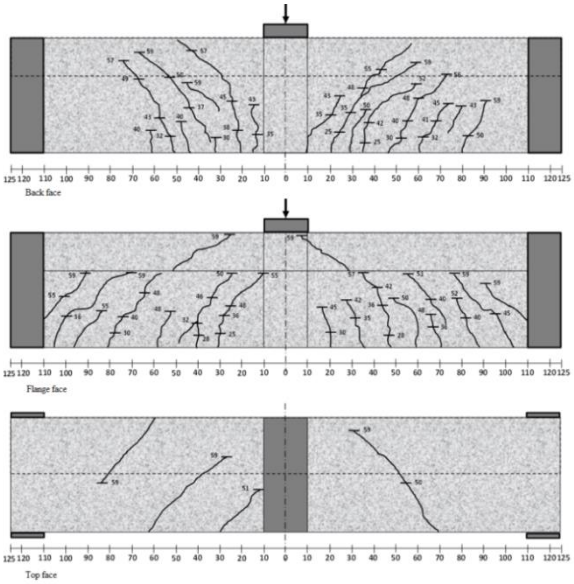

Fig. 18 Crack pattern in beam S1.5-545

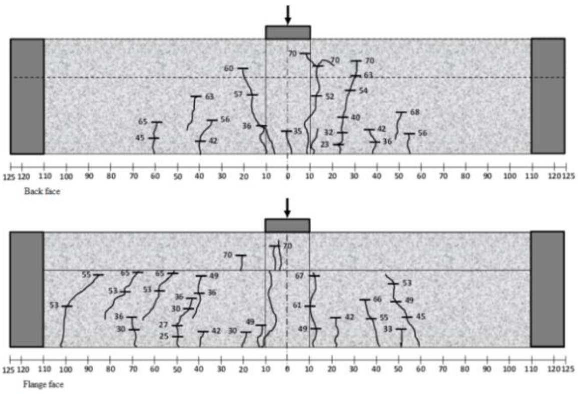

Fig. 19 Crack pattern in beam S1-145

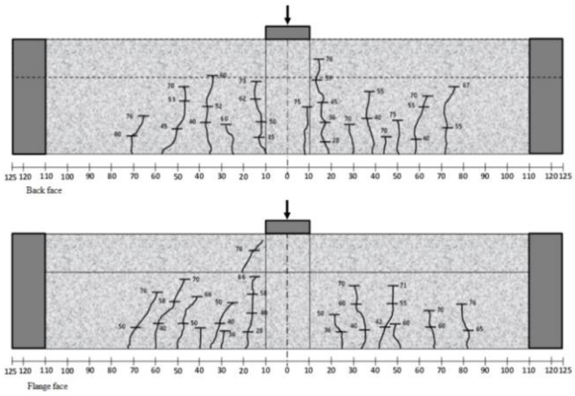

Fig. 20 Crack pattern in beam S1.5-145

The addition of steel fibers did not change the crack pattern, but a slight increase in these numbers was observed for the two loading cases.

Beams S1-545 and S1.5-545 cracked on two vertical faces at P_{cr}=0.38 $P_{\max}$ and P_{cr}=0.42 $P_{\max}$, respectively. Before torsional failure, the top faces cracked at 0.86 $P_{\max}$ and 0.85 $P_{\max}$, respectively (Figs. 17 and 18, respectively).

Specimens tested under low eccentricity and reinforced by 1.0% and 1.5% volume fraction of steel fibers, respectively, had crack patterns similar to those of the plain beam (without fibers). Beam S1-145 cracked on the back face at P_{cr}=0.33 $P_{\max}$ and on the flange face at 0.36 $P_{\max}$ (Fig. 19). When the ratio of steel fibers increased to 1.5% in beam S1.5-145, the back and flange faces cracked at P_{cr}=0.37 $P_{\max}$ (Fig. 20). For two steel volume ratios, the bending failure was controlled as indicated by vertical cracks.

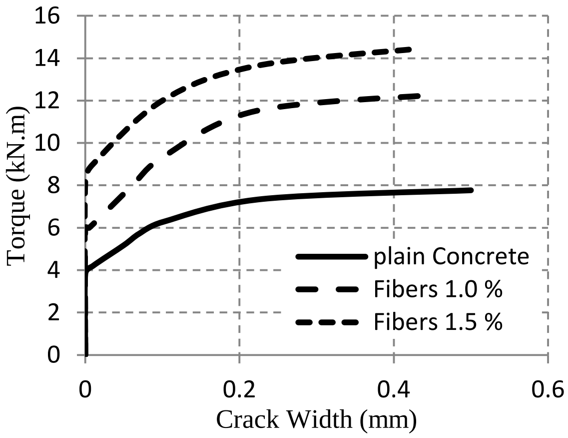

Fig. 21 Torque-crack width curve of the back face of beams in Group I under *e*=545 mm

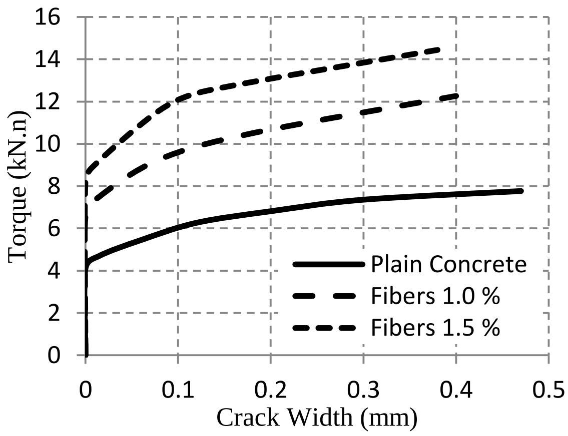

Fig. 22 Torque-crack width curve of the flange face of beams in Group I under *e*=545 mm

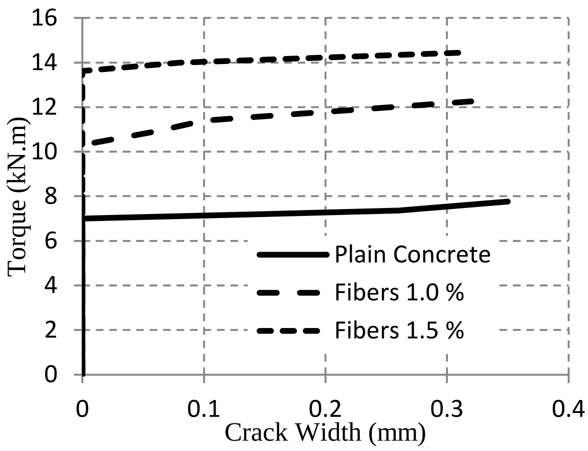

Fig. 23 Torque-crack width curve of the top face of beams in Group I under *e*=545 mm

3.3 Crack width and spacing

All specimens were painted in white to make the fine cracks visible at the beginning and to accurately detect the cracking load. After each load step, the two vertical sides of the specimens were observed carefully using a flashlight, and the crack width was measured using a crack microscope.

For beams in Group I under *e*=545 mm, the crack widths increased with increasing load level. However, when the top face started to crack, crack width increased largely in two vertical faces until failure. The same behavior was observed on the back and flange sides (Figs. 21 and 22, respectively). The crack spacing for these two vertical faces ranged from150 mm to 350 mm. The top face crack width was almost linear (Fig. 23).

Under low eccentricity, crack width was less than that under high eccentricity. The spacing on two vertical faces ranged from 150 mm to 200mm (Fig. 24 and 25, respectively).

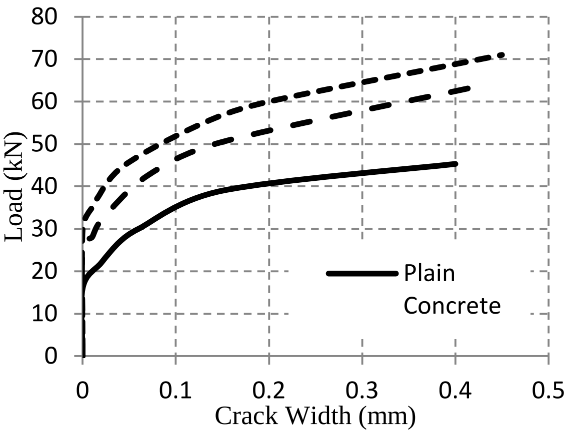

Fig. 24 Load-crack width curve of the back face of beams in Group I under e=145 mm

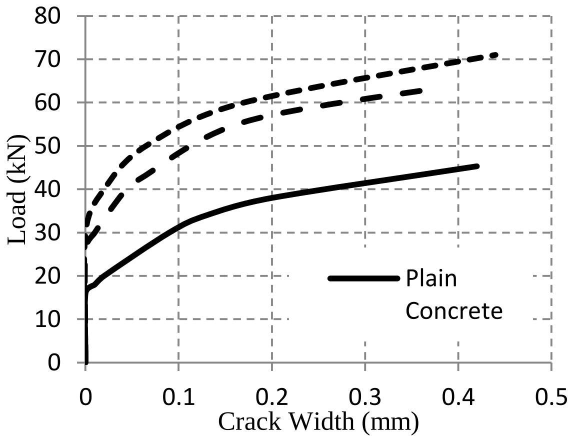

Fig. 25 Load-crack width curve of the flange face of beams in Group I under e=145 mm

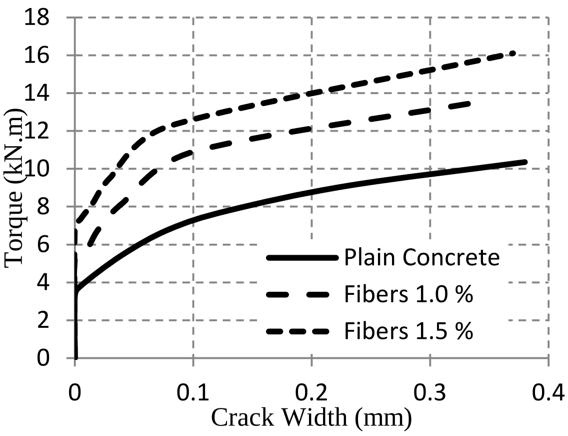

Fig. 26 Torque-crack width curve of the back face of beams in Group II under e=545 mm

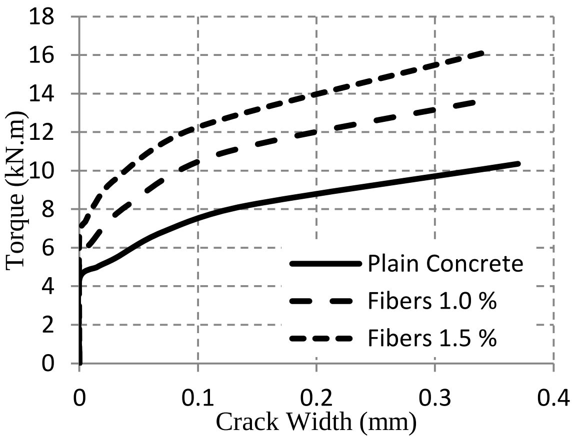

Fig. 27 Torque-crack width curve of the flange face of beams in Group II under e=545 mm

The addition of steel fibers restricted the development of crack width to a great extent. The cracking load value increased, and the crack width was very small compared with that of plain concrete until the crack appeared on the top face (near the max load). When the steel fibers yielded, the cracks widened quickly. The same behavior also appeared on the flange side of the beam. The top face was not affected by the addition of fiber. The spacing was reduced to the range of 90 mm to 150 mm for 1.5% steel fiber volume fraction under e=545 mm. The spacing was also reduced to the range of 100 mm to 150 mm for 1.5% volume fraction under e=145 mm.

The addition of transverse reinforcement for the beams in Group II reduced the crack width unlike that for the beams in Group I in high and low torsion. The spacing ranged from 150 mm to 200 mm for beam under high eccentricity. Crack spacing for beams under low eccentricity ranged from 100 mm to 200 mm (Figs. 26 and 27, respectively).

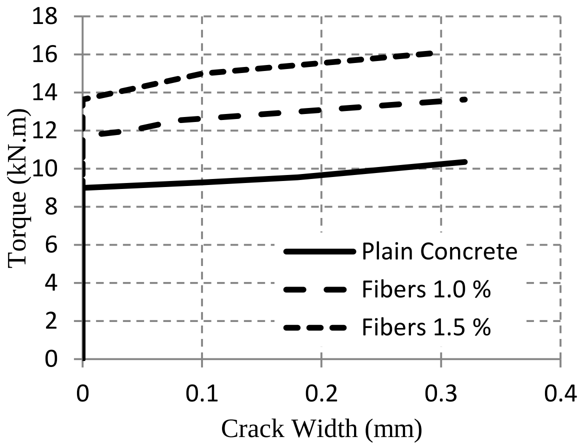

Fig. 28 Torque-crack width curve of the top face of beams in Group II under *e*=545 mm

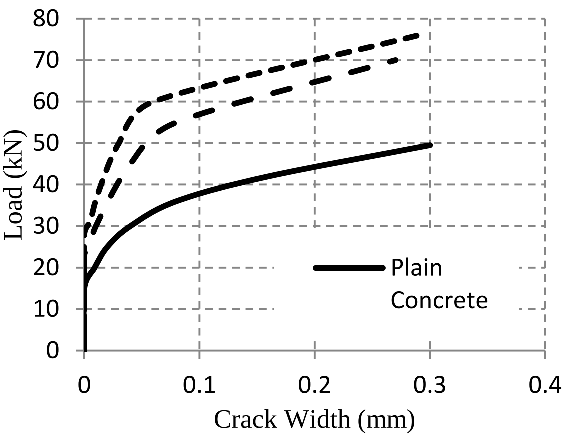

Fig. 29 Load-crack width curve of the back face of beams in group II under *e*=145 mm

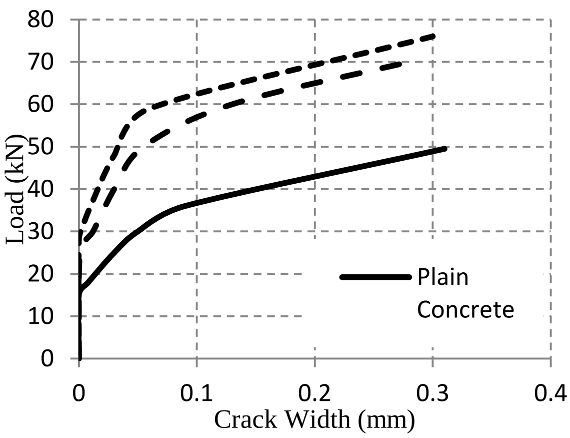

Fig. 30 Load-crack width curve of the flange face of beams in group II under *e*=145 mm

Steel fibers also reduced the crack width value to a good percentage. The back and flange sides behaved similarly under two loading conditions, and the top face behaved linearly (Fig. 28). The spacing was reduced to the range of 50 mm to 100 mm for high eccentricity after 1.5% steel volume fraction was added. Spacing that ranged from mm 50 to 150 mm was noted for low eccentricity (Figs. 29 and 30).

3.4 Strain in concrete

Strain on the concrete surface was measured at mid-span on the back face of a beam. A strain gauge was fixed at mid-depth, horizontal, and inclined at 45°. The readings were recorded at all load steps.

As expected, the generation of cracks significantly affected the strain values. A quick increase was observed after the crack occurred (Rahal and Collins 2006).

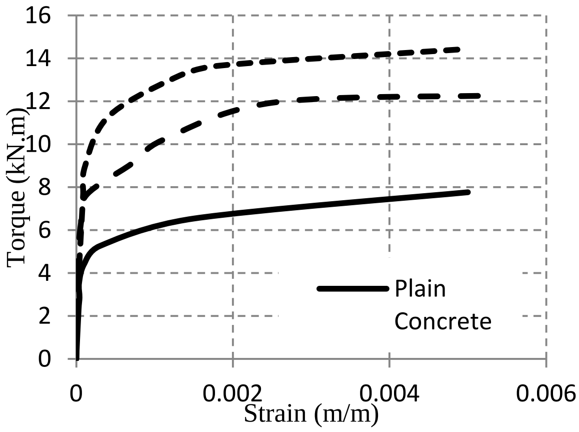

Fig. 31 Torque-strain curve for beams in Group I under *e* =545 mm (0° strain)

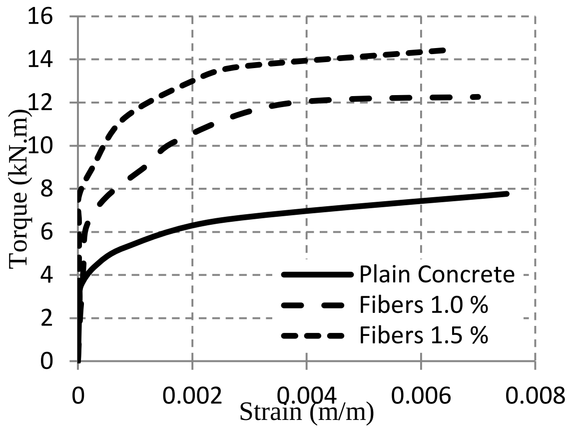

Fig. 32 Torque-strain curve for beams in Group I under *e*=545 mm (45° strain)

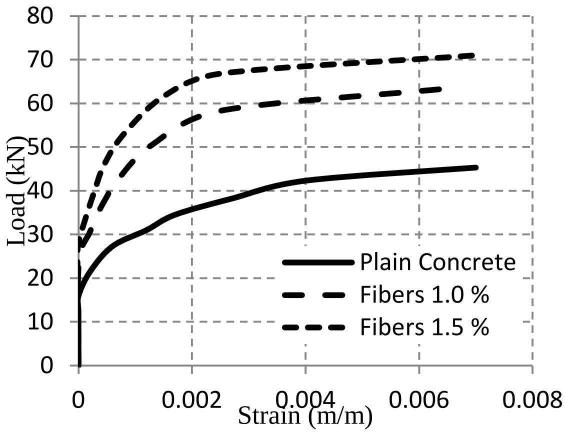

Fig. 33 Load-strain curve for beams in Group I under *e*=145 mm (0° strain)

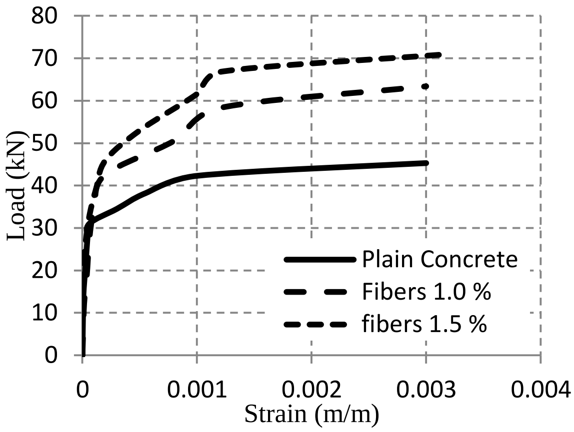

Fig. 34 Load-strain curve for beams in Group I under *e*=145 mm (45° strain)

The general behavior was similar to that of the crack width. Figs. 31 and 32 show the strain values at mid-span of a beam measured by horizontal and inclined strain gauges, respectively, under a high torsion value for Group I specimens. Steel fiber addition decreased the strains by limiting the crack width.

At low eccentricity, the horizontal strain had larger values than the inclined one, and all the strains were tensile strains (Figs. 33 and 34).

Stirrups also reduced the strains especially at a high eccentricity (*e*) value for beams in Group II. The same general behavior of strain values for Group I specimens was noted for this group, but the values decreased because of the stirrups (Figs. 35 and 36).

The increase in volume fraction of fibers had a minor effect on *e*=145 mm compared with that on *e*=545 mm (Figs. 37 and 38).

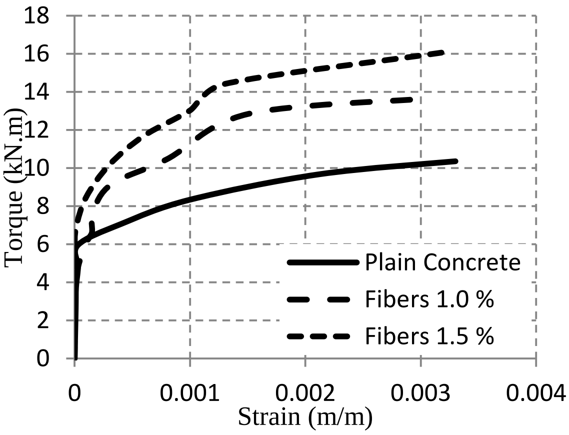

Fig. 35 Torque-strain curve for beams in Group II under *e*=545 mm (0° strain)

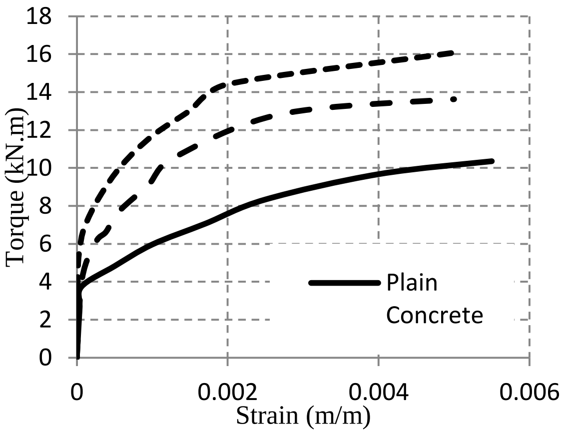

Fig. 36 Torque-strain curve for beams in Group II under *e*=545 mm (45° strain)

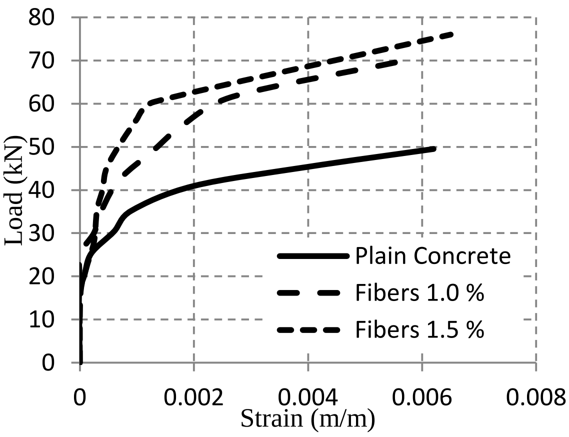

Fig. 37 Load-strain curve for beams in Group II under *e* =145 mm (0° strain)

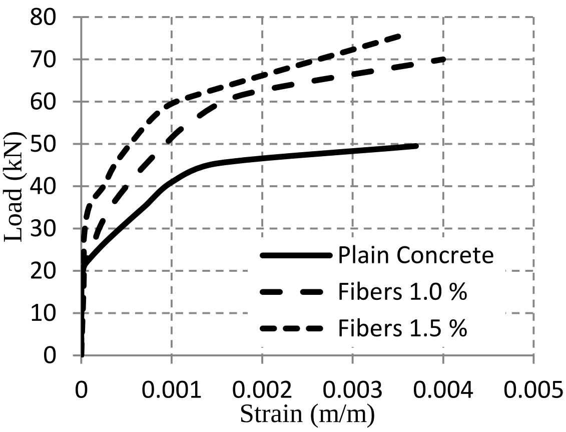

Fig. 38 Load-strain curve for beams in Group II under *e*=145 mm (45° strain)

4. Conclusions

• Crack pattern development in beams depends mainly on the torque to shear ratio (eccentricity).

• Angle of cracks increased by addition steel fibers under high torsion value for specimens with and without stirrups.

• Crack width was reduced by steel fiber addition, and the concrete surface strain was reduced as well.

• The same number of cracks appeared on two vertical faces of the beams at high and low torsion value.

• The back face of the beam cracks before the flange face at high torsion value.

• The addition of steel fibers improved the overall strength of L-shaped beams with respect to the non-fibrous control specimens, particularly of beams under high eccentricity.

References

ACI 318-05 (2005), American concrete institute, Building code requirements for reinforced concrete, Farmington Hills, Michigan.

ACI Committee 544 (1999), American Concrete Institute, Design considerations for steel fiber reinforced concrete, ACI manual of concrete practice, Farmington Hills.

Avinash, S.P. and Parekar, R.S. (2010), "Steel fiber reinforced concrete beams under combined torsion-bending-shear", *J. Civil Eng*., **38**(1), 31-38.

Chalioris, C.E. and Karayannis, C.G. (2009), "Effectiveness of the use of steel fibers on the torsional behavior of flanged concrete beams", *Cement Concrete Compos.*, **31**, 331- 341.

Craig, R.J., Parr, J.A., Germain, E., Mosquera, V. and Kamilares, S. (1986), "Fiber-reinforced beams in torsion", *ACI J.*, **83**(6), 934-942.

Deifalla, A. and Ghobarah, A. (2010), "Strengthening RC T-beams subjected to combined torsion and shear using FRP fabrics: experimental study", *J. Compos. Constr.*, **14**(3), 301-311.

El-Niema, E.I. (1993), "Fiber reinforced concrete beams under torsion", *ACI Struct. J.*, **90**(5), 489-495.

Gunneswara Rao, T.D. and Rama Seshu, D. (2003), "Torsion of steel fiber reinforced concrete members", *Cement Concrete Res.*, **33**, 1783-1788.

Gunneswara Rao, T.D. and Rama Seshu, D. (2005), "Analytical model for the torsional response of steel fiber reinforced concrete members under pure torsion", *Cement Concrete Compos.*, **27**, 493-501.

Hsu, T.T.C. (1984), *Torsion of Reinforced Concrete*, Van Nostrand Reinhold, New York.

Mansur, M.A. and Paramasivam, P. (1982), "Steel fiber-reinforced concrete beams in pure torsion", *Int. J. Cement Compos. Lightw. Concrete*, **4**(1), 39-45.

Mansur, M.A. and Paramasivam, P. (1985), "Steel fiber reinforced concrete beams in torsion, bending and shear", *ACI J.*, **82**(1), 33-39.

Narayanan, R. and Kareem-Palanjian, A.S. (1986), "Torsion in beams reinforced with bars and fibers", *J. Sruct. Eng.*, ASCE, **112**(1), 53-66.

Newman, J. and Choo, B.S. (2003), *Advance Concrete Technology*, 1st Edition, Elsevier, London.

Okay, F. and Engin, S. (2012), "Torsional behavior of steel fiber reinforced concrete", *Constr. Build. Mater.*, **28**, 269-275.

Rahal, K.H. and Collins, M.P. (2006), "Compatibility torsion in spandrel beams using modified compression field theory", *ACI Struct. J.*, **103**(3), 328-338.

Wafa, F.F., Hasnat, A. and Tarabolsi, O.F. (1992), "Prestressed fiber-reinforced concrete beams subjected to torsion", *ACI Struct. J.*, **89**(3), 272-283.

Wight, J.K. and MacGregor, J.G. (2009), *Reinforced Concrete: Mechanics and Design*, Pearson Prentice Hall, New Jersey, USA.

Zararis, P.D. and Penelis, G. Gr. (1986), "Reinforced concrete T-beams in torsion and bending", *ACI J.*, **83**, 145-154.

CC